

The evolution mechanism of FeMo alloy catalyst for growth of single-walled carbon nanotube

Xuan Chen,^a Haiming Duan,^{a,b}* Biaobing Cao^a, Qihua Sun^a and Wenhui Yang^a

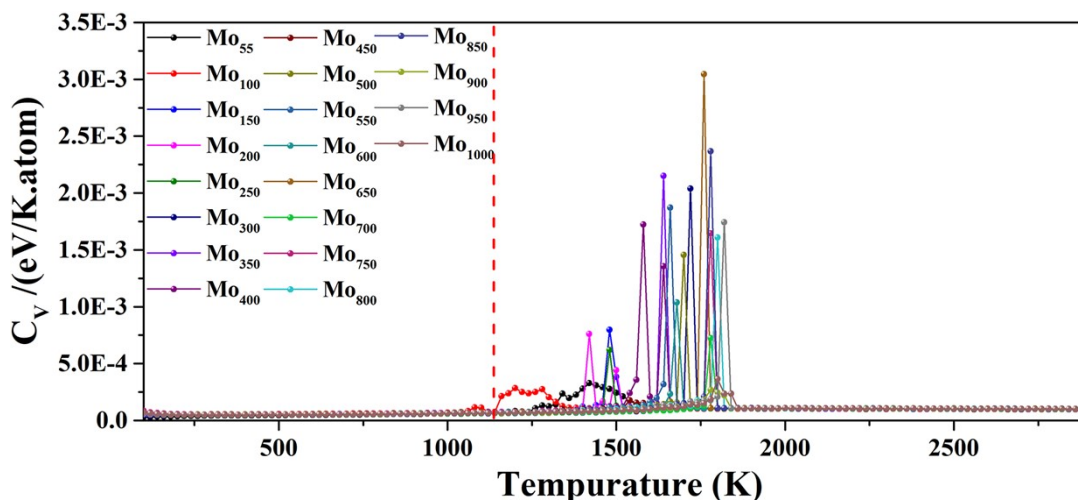
^aSchool Of Physical Science And Technology. Xinjiang University, Urumqi 830046, People's Republic of China

^bXinjiang Key Laboratory of Solid State Physics and Devices, Xinjiang University, Urumqi, 830046, China

Table content

Figure S1	3
Figure S2	4
Figure S3	5
Figure S4	8
Figure S5	9
Figure S6	10
Reference.....	11

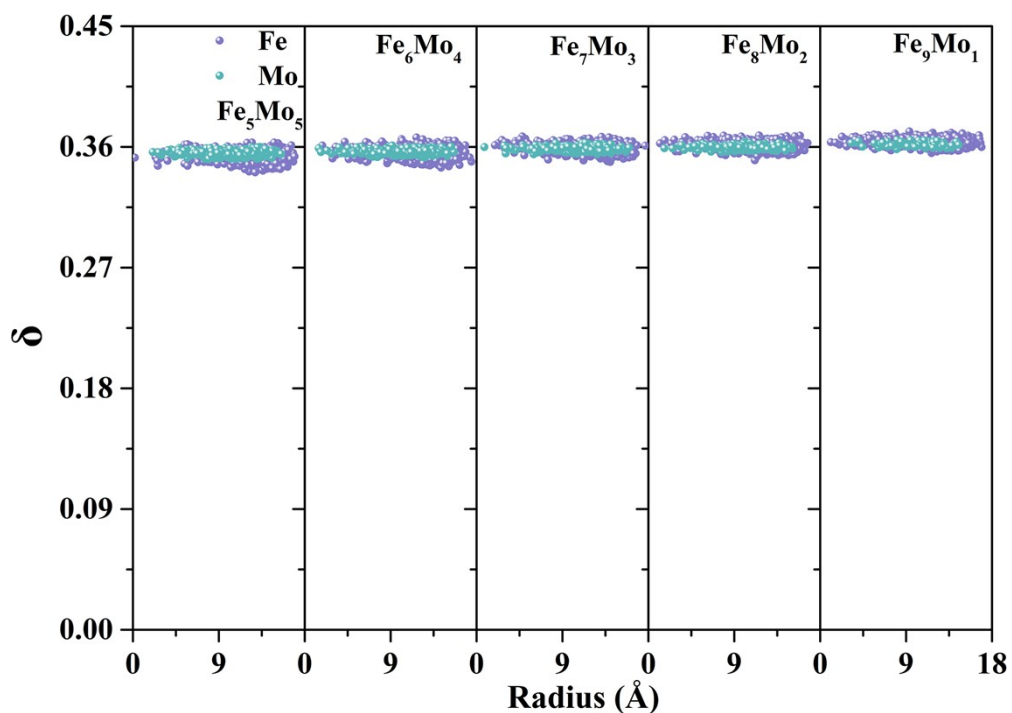
Figure S1 The heat capacity (C_v) of a typical MD heating process of Mo NP with different sizes, the black dash line represents about 1125K.



The melting point of Mo was reported by Gohil¹ by using the classical molecular dynamics with the Gupta potential with the parameter from Ref. 2. The result was in agreement with the experimental and ab initio MD finds. To further compare the melting point of the Mo cluster in simulation with experiments^{3,4}, we investigated the melting point of the Mo cluster with different sizes.

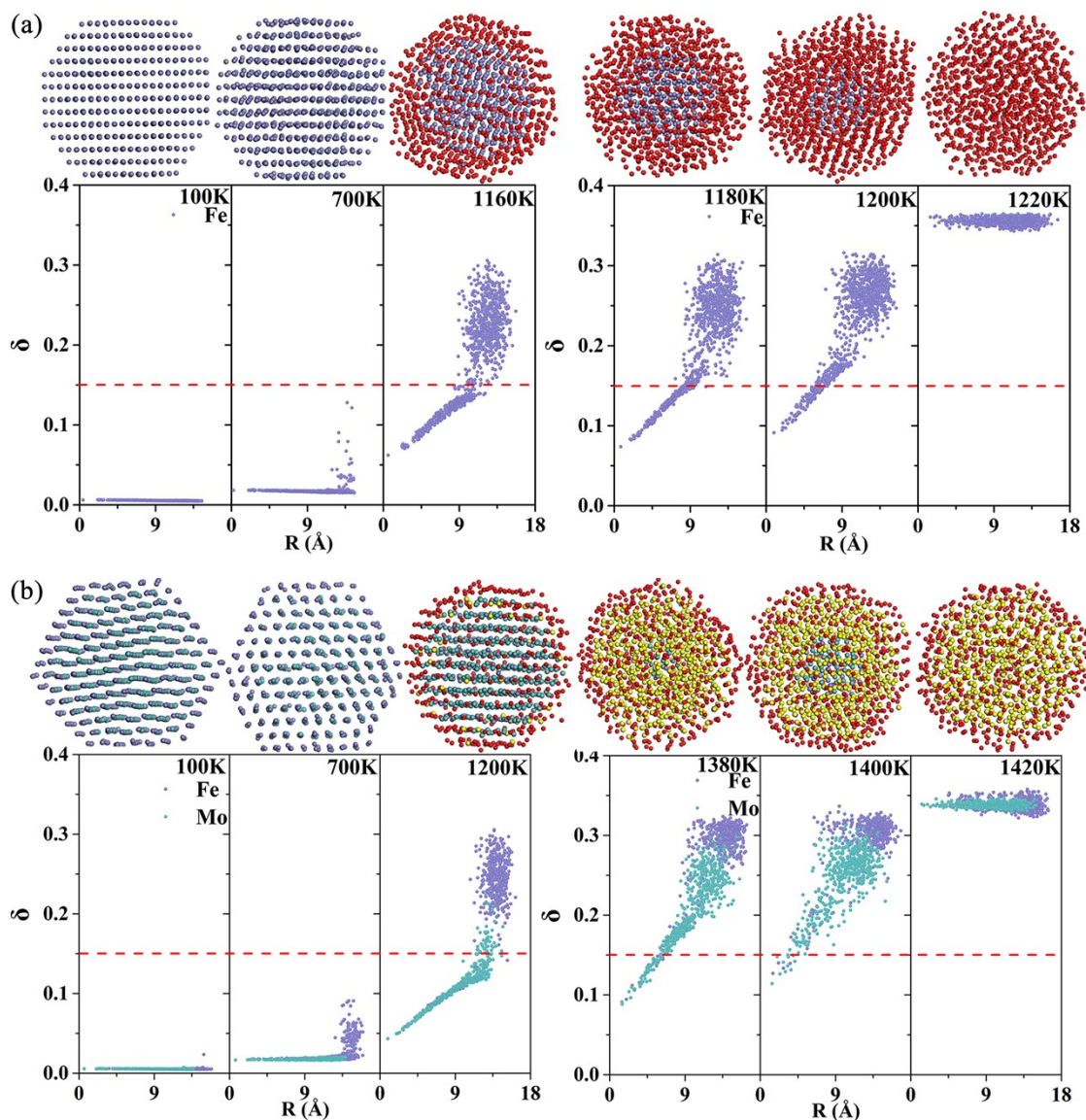
According to the experimental results^{3,4}, Mo catalysts will first combine with C, then convert to the Mo₂C to promote the growth of SWCNT via vapor-solid-solid model at the 850°C (approximately 1125K) in chemical vapor deposition reaction. In the above process, the Mo catalyst does not undergo the common “re-shaping” process⁴ i.e., the melting point of the Mo NP, whose diameter is large than or equal to 1 nm, is higher than 1125K, at least. Hence, to compare the melting point of Mo NP between the experiment and simulation. Figure S1 presents the heat capacity of a typical MD heating process of Mo NP with different sizes. Although the melting point of the part of Mo NPs can't be precisely defined through the abrupt peak of heat capacity, the melting point of all Mo NPs is higher than 1125 K (the red dash line in figure S1).

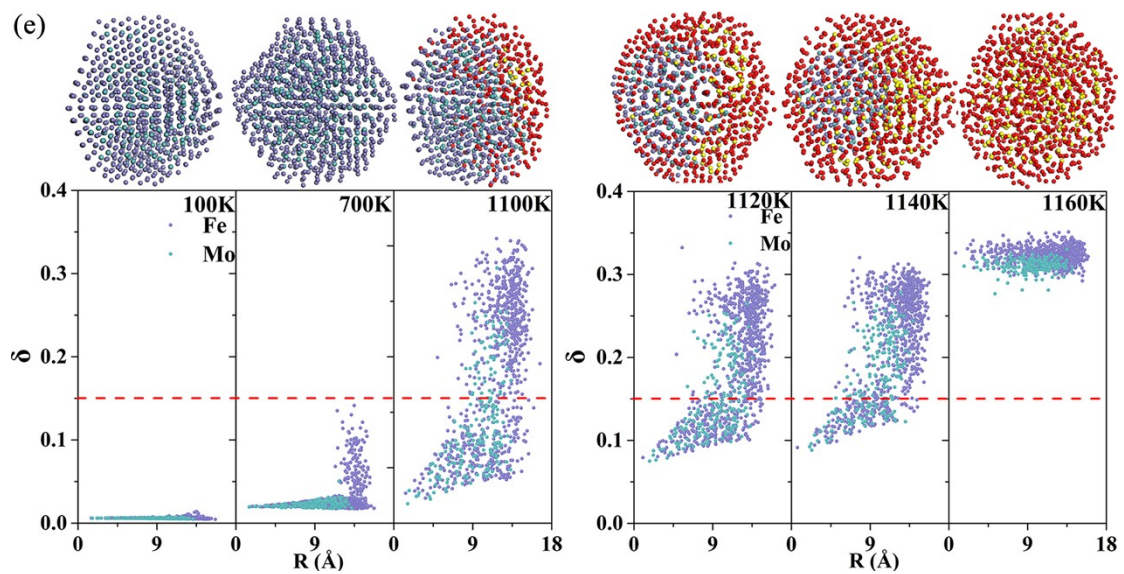
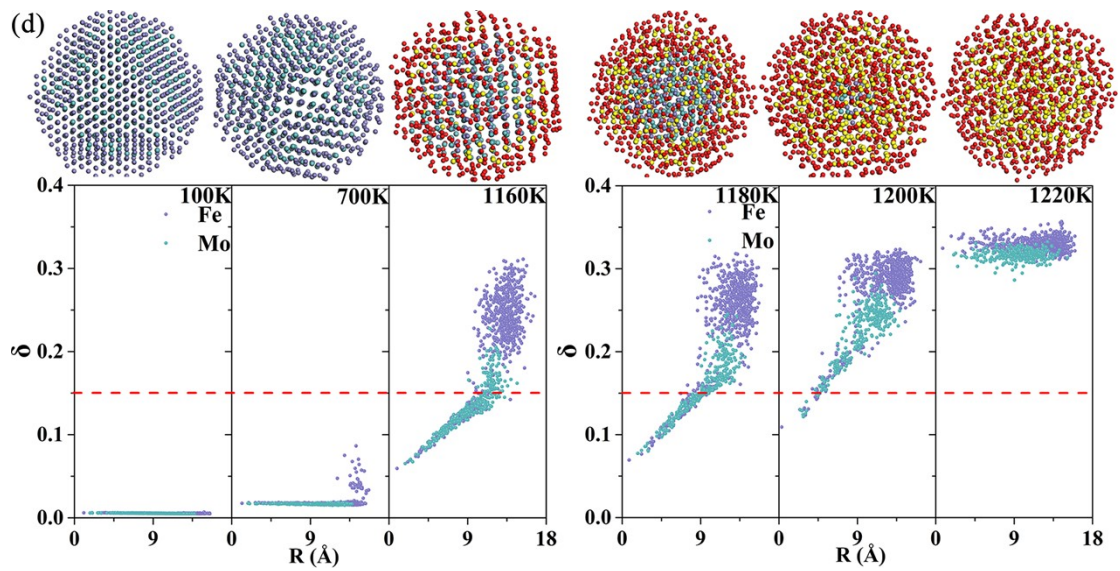
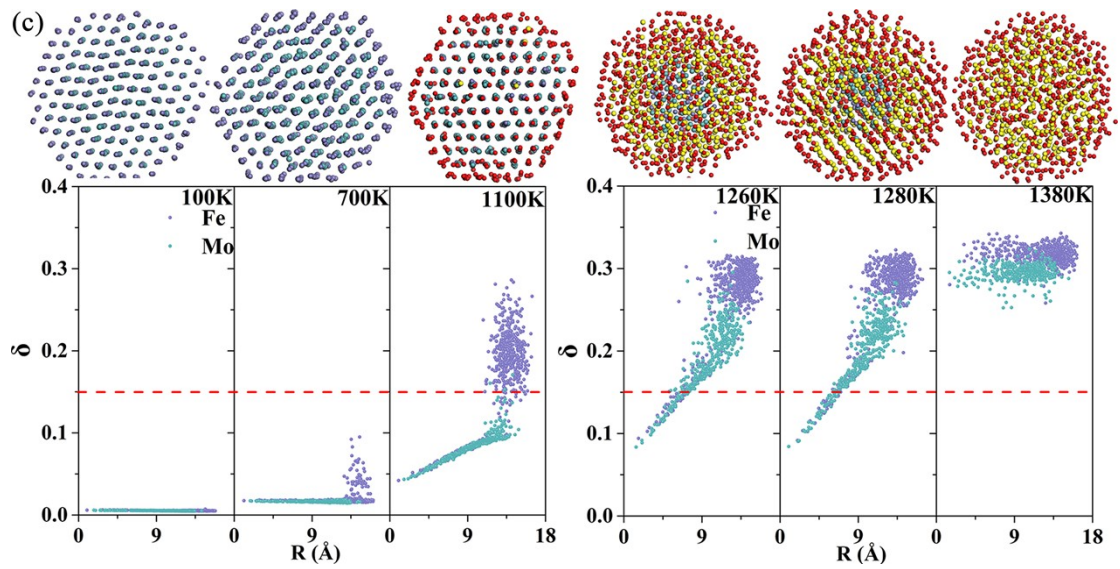
Figure S2 Lindemann index variation of different type atoms in (a) Fe_5Mo_5 , (b) Fe_6Mo_4 , (c) Fe_7Mo_3 , (d) Fe_8Mo_2 and (e) Fe_9Mo_1 NP at 1000K.

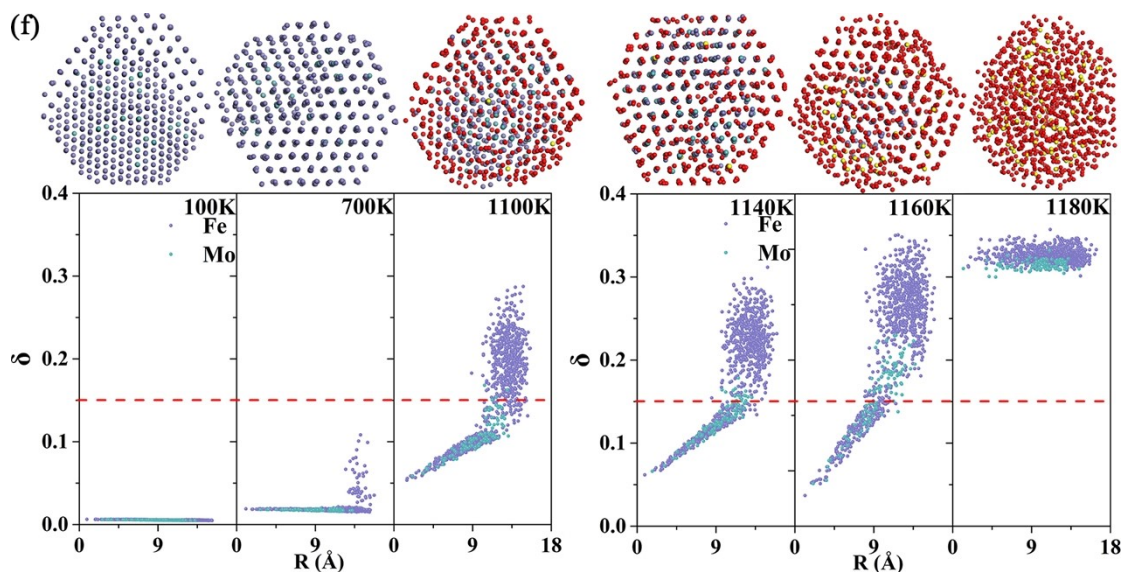


As figure S2 presents, we investigated the atomic Lindemann index of FeMo NPs at 1900K. All atomic Lindemann indexes in FeMo NP are higher than 0.33 at 1900K. In other words, all FeMo NP is a “liquid” state at this temperature. So, we believe that the temperature ranging of annealing simulations to obtain the EMS of FeMo NPs is reasonable.

Figure S3 Atomic lindemann index variation of (a) Fe, (b) Fe₅Mo₅, (c) Fe₆Mo₄, (d) Fe₇Mo₃, (e) Fe₈Mo₂ and (f) Fe₉Mo₁ NP at different temperatures. The light purple and green dots are corresponding to Mo and Fe atoms, and the light purple or green (red and yellow) balls in the snapshot is the Fe (Mo) atom, in which the Lindemann index is lower or higher than 0.15. Note that the radius denotes the distance of the atom from the center of the particle.







From figure S3, we see that the melting behavior of Fe_8Mo_2 is different from others. As illustrated in figure S3 (e), the Lindemann index of Fe atoms on the surface of Fe_8Mo_2 NP is different. More precisely, because of the larger deformation parameter of Fe_8Mo_2 (see figure S5) to lead the Fe atoms, which are located on one side of the surface of Fe_8Mo_2 NPs, are easily activated than the other side of Fe atoms. Then, those active atoms can transfer their higher energy to adjacent atoms, that are located at the subsurface or on the surface of NP to activate them. At the same time, the atoms on the other side of the NP still keep the lower Lindemann index. Furthermore, as the temperature increases, although, the number of active atoms on the surface of the NP continuously increases, it still can be distinguished by the number of active atoms on one side of the NP being larger than on the other side (figure S3 (e)). Then more atoms that are linked with more active atoms can be activated. Therefore, the gap between the atomic Lindemann index, with the same distance from the mass center, of the Fe_8Mo_2 becomes gradually narrow (see figure S3 (e)), until the temperature reaches 1160 K.

Figure S4 Temperature dependence of diffusion coefficients for (a) Fe and (b) Mo in Fe, Fe₅Mo₅, Fe₆Mo₄, Fe₇Mo₃, Fe₈Mo₂, and Fe₉Mo₁ NP.

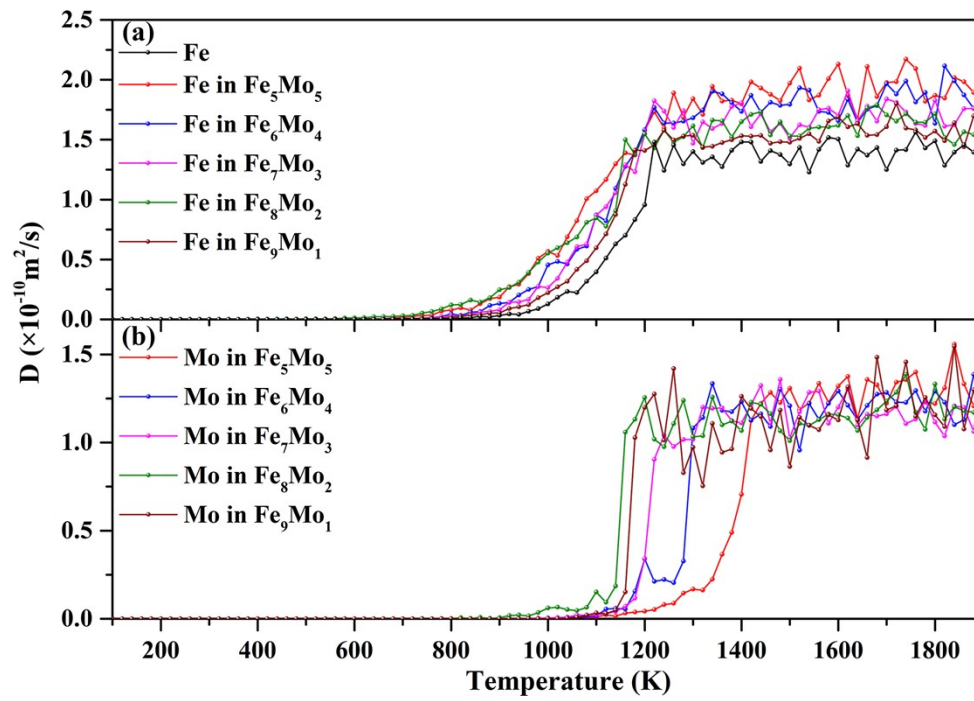
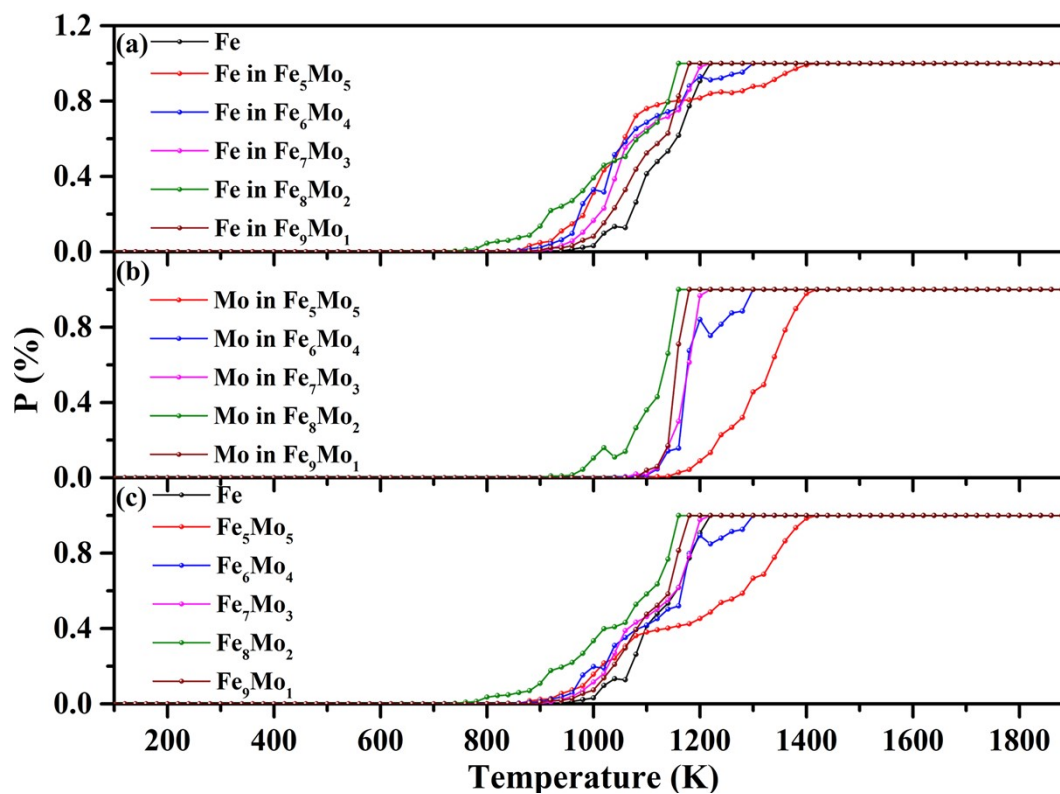


Figure S5 Percentage of active (a) Fe (b) Mo and (c) total atoms in the heating process.



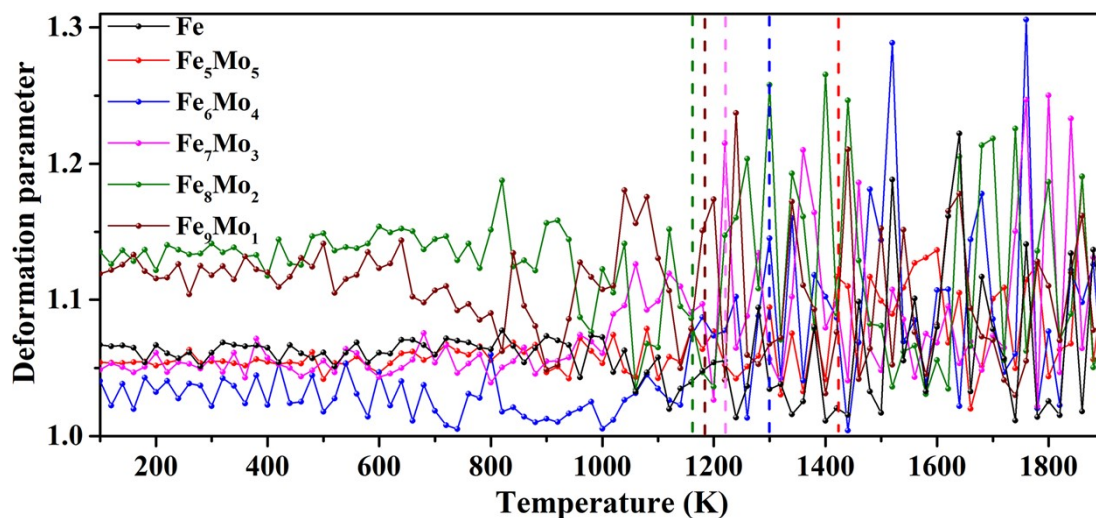
We define the percentage of active atoms in the NP as follows

$$P_{metal} (\%) = \frac{N_{metal_a}}{N_{metal_t}} \times 100\%$$

Where N_{metal_a} or N_{metal_t} is the number of active or total atoms of the target metal, respectively.

The percentage of different types of active atoms in the heating process is presented in figure S5.

Figure S6 The shape evolution of FeMo NP as a function of temperature.



When analyzing figure S6, the deformation parameters of all NPs were larger than 1, i.e., the shape of the NP deviates from the standard sphere. Then, the fluctuation of the deformation parameter of NP becomes gradually violent in the heating process. This is attributed to the following reasons: first, the surface pre-melting of NP occurs at a lower temperature. Then the active atoms that are not fixed at a certain place can lead to the minor fluctuation of the deformation parameter. Then as the temperature increases more atoms get activated, so the fluctuation of the deformation parameter gradually intensifies. Finally, the order of the atoms in the NPs is destroyed when the temperature is higher than the melting point of NPs. Then to cause the NPs is a liquid droplet-like configuration with no fixed shape.

To further compare the deformation parameter of NPs, the deformation parameter of Fe₈Mo₂ is higher than other NPs. In other words, Fe₈Mo₂ tends to be more ellipsoid-like in structure than other NPs, such as Fe₇Mo₃, Fe₆Mo₄, Fe₅Mo₅, and Fe₉Mo₁ NPs. This caused the Fe₈Mo₂ with longer Fe-Fe, Fe-Mo bond, higher atomic diffusion coefficients, and larger percentage of active atoms, even higher than Fe₇Mo₃.

Reference

1. D. R. Gohil, N. K. Bhatt, A. B. Patel and P. R. Vyas, *AIP Conf. Proc.*, 2021, **2352**, 020036.
2. M. A. Karolewski, *Radiat. Eff. Defects Solids*, 2001, **153**, 239 – 255.
3. S. C. Zhang, L. X. Kang, X. Wang, L. M. Tong, L. W. Yang, Z. Q. Wang, K. Qi, S. B. Deng, Q. W. Li, X. D. Bai, F. Ding and J. Zhang, *Nature*, 2017, **543**, 234 - 238.
4. X. Zhang, B. Graves, M. D. Volder, W. M. Yang, T. Johnson, B. Wen, W. Su, R. Nishida, S. S. Xie and A. Boies, *Sci. Adv.*, 2020, **6**, eabb6010.